J.L. Santiago, F. Martín, A. Cuerva, N. Bezdenejnykh, A. Sanz-Andrés

Experimental and numerical study of wind flow behind windbreaks

Abstract

The shelter effect of a windbreak protects aggregate piles and provides a reduction of particle emissions in harbours. RANS (Reynolds-averaged Navier–Stokes equations) simulations using three variants of k–ε (standard k–ε, RNG k–ε and realizable k–ε) turbulence closure models have been performed to analyse wind flow characteristics behind an isolated fence located on a flat surface without roughness elements. The performance of the three turbulence models has been assessed by wind tunnel experiments. Cases of fences with different porosities (ϕ) have been evaluated using wind tunnel experiments as well as numerical simulations. The aim is to determine an optimum porosity for sheltering effect of an isolated windbreak. A value of 0.35 was found as the optimum value among the studied porosities ($\phi = 0$, 0.1, 0.24, 0.35, 0.4, 0.5).

1. Introduction

Large amounts of materials in aggregate form are handled, stored and transported in harbour areas producing important particle emissions to the environment. These materials existing in harbours are usually stored piled up on ground in an open location. The open storage produces dust emission from aggregate piles, wind erosion being the main factor of the emissions. These emissions should be controlled and reduced as much as possible and a way to diminish them is to use windbreaks to protect the piles from wind erosion (Borges and Viegas, 1988; Jensen et al., 2001).

The windbreak objective is to provide a shelter effect by decreasing the wind speed in a large zone behind the fence. Depending on barrier characteristics, different wind speed reductions and turbulence features are found in different leeward areas. Porosity, defined as the ratio between the area of the holes and the total area of the fence, is considered as the most influential parameter in the flow pattern behind a windbreak (Perera, 1981). A no re-circulating flow zone behind the windbreak is found when the porosity is higher than 30% (Perera, 1981). Several empirical relationships link the value of the fence resistance coefficient (defined in Section 2.2)

with the windbreak porosity (Reynolds, 1969; Perry et al., 1997; Lee and Lim, 2001). The ratio h_b/z_0, where h_b is the height of the barrier and z_0 is the roughness length around the windbreak, is also important, especially for modelling purposes (Raine and Stevenson, 1977; Judd et al., 1996).

The literature is rich with studies on windbreak flow with both experiments and numerical simulations. For example, windbreak aerodynamics was reviewed by Plate (1971) and measurements of mean velocity and turbulence variables behind single solid and porous fences were carried out by Raine and Stevenson (1977). The authors found a protection zone for medium porosity fences larger than that for solid windbreaks. In addition, many numerical studies on flow with shelterbelts have been carried out. An early work was made by Tani (1958) where windbreak was treated as a source of momentum deficit, which was considered as a scalar controlled by turbulent diffusion. More complex models have been used with the advent of growing computational power. Wilson (1985) used Reynolds-averaged Navier–Stokes (RANS) equation introducing a momentum sink involving the fence resistance coefficient to simulate a porous barrier. His results showed a quite good prediction of the flow pattern near a single porous windbreak, but further downwind underestimated the rate of return towards the upstream equilibrium. Similar simulations are carried out by Wang and Takle (1995) and Wilson and Mooney (1997). Wang and Takle (1995) did not find the previous problem outlined by Wilson (1985), and Wilson and Mooney (1997) proposed that the reason may be the computational domain size used (too shallow for Wang and Takle, 1995). RANS model inaccuracy in this context has been analysed by Wilson and Yee (2003) and Wilson (2004b). Higher inaccuracy were found in complex cases, as the wind over a windbreak array (data of McAneney and Judd, 1991 case) or the oblique and stratified winds around a shelterbelt (data of Wilson, 2004a case). They found that the RANS models produce an ambiguity in their results due to the choice of the turbulent closure and the discretisation error. They concluded that a balanced view of the problem is the reassessment of both testing closure models and schemes in order to determine the potential value of RANS models and to avoid the premature substitution of measurements for models. For this reason, one part of this study is devoted to perform the comparison of three different turbulence models with the same numerical procedure and parameters (same domain, grid, boundary conditions, etc.) focusing on the differences due to the performance of the turbulence and leaving aside the effects of other factors (grid, boundary conditions, etc.). Other more complex models such as large-eddy simulations (LES) have also been applied. For example, Patton et al. (1998) used LES to simulate turbulent flow field around multiple windbreaks within a homogeneous plant canopy.

This paper is focused on the shelter effect of windbreaks located in harbour areas. In these areas, the fences are used for protecting aggregate piles stored in open locations, and therefore the wind profiles impinging the fences are characterised by roughness lengths corresponding to sea or flat coastal zones which have very low values (10^{-3}–10^{-4} m) as pointed out by Dyrbye and Hansen (1997) and Gao et al. (2000). To obtain such flat profile the wind tunnel experiments have been carried out without roughness elements obtaining streamwise velocity profiles which corresponds to a z_0 close to 0 (see Section 4.1) (even if roughness length can never reach 0, obviously). The shelter effect of an isolated windbreak depends on its porosity, and this paper aims to determine its optimum value giving rise to the largest shelter zone in the above mentioned conditions. Thus, wind flow around isolated windbreaks is studied by means of wind tunnel experiments and numerical simulations for a range of porosities from 0 (solid fence) to 0.5. The experiments have been carried out in the A9 wind tunnel of IDR/UPM, E.T.S.I. Aeronáuticos, Universidad Politécnica de Madrid and the numerical simulations have been performed by a RANS model using different variant of k–ε turbulence closure: standard k–ε, RNG k–ε and realizable k–ε. Thus, each turbulence model results have been compared against wind tunnel data and their influence on the final results has been analysed in the turbulence models. All the other characteristics of the numerical method (grid, domain, etc.) have been maintained identical.

2. Numerical methods

FLUENT CFD software was used to simulate wind flow patterns around windbreaks.

2.1. Governing equations

The simulations are based on Reynolds-averaged Navier–Stokes equations (RANS) using three different

turbulence closure models (standard k–ε, RNG-k–ε and realizable k–ε). Four types of equations are solved in each case: continuity equation (1), RANS equations (2), and two turbulence closure equations (3)–(4) for standard k–ε; 5–6 for RNG k–ε; 7–8 for realizable k–ε) for the turbulent kinetic energy (k) and for the dissipation rate of turbulent kinetic energy (ε), respectively:

$$\frac{\partial u_j}{\partial x_j} = 0, \tag{1}$$

$$\frac{\partial u_i}{\partial t} + u_j \frac{\partial u_i}{\partial x_j} = -\frac{1}{\rho}\frac{\partial p}{\partial x_i} + \frac{\mu}{\rho}\frac{\partial^2 u_i}{\partial x_j \partial x_j} - \frac{\partial}{\partial x_j}(\overline{u_i' u_j'}) + g_i, \tag{2}$$

$$\frac{\partial k}{\partial t} + u_j \frac{\partial k}{\partial x_j} = \frac{1}{\rho}\frac{\partial}{\partial x_j}\left[\left(\mu + \frac{\mu_t}{\sigma_k}\right)\frac{\partial k}{\partial x_j}\right] + \frac{G_k}{\rho} - \varepsilon, \tag{3}$$

$$\frac{\partial \varepsilon}{\partial t} + u_j \frac{\partial \varepsilon}{\partial x_j} = \frac{1}{\rho}\frac{\partial}{\partial x_j}\left[\left(\mu + \frac{\mu_t}{\sigma_\varepsilon}\right)\frac{\partial \varepsilon}{\partial x_j}\right] + \frac{1}{\rho} C_{\varepsilon 1} G_k \frac{\varepsilon}{k} - C_{\varepsilon 2}\frac{\varepsilon^2}{k}, \tag{4}$$

where u_j is the j component of velocity, t is the time, x_j is the j coordinate, ρ is the air density, μ is the dynamic viscosity; g_i is the gravitational body force;

$$-\overline{u_i' u_j'} = \frac{1}{\rho}\mu_t\left(\frac{\partial u_i}{\partial x_j} + \frac{\partial u_j}{\partial x_i}\right) - \frac{2}{3}k\delta_{ij}$$

is the Reynolds stress; $\mu_t = \rho C_\mu k^2/\varepsilon$ is the turbulent viscosity; G_k is the turbulent kinetic energy production; σ_k (= 1.0) and σ_ε (= 1.3) are turbulent Prandtl number for k and ε, respectively; C_μ, $C_{\varepsilon 1}$ and $C_{\varepsilon 2}$ are model constants ($C_\mu = 0.09$; $C_{\varepsilon 1} = 1.44$; $C_{\varepsilon 2} = 1.92$). These values of model constants are shown as the most suitable for a wide range of turbulent flows (Launder and Spalding, 1974; Versteeg and Malalasekera, 1995).

RNG k–ε is based on RNG theory (Yakhot and Orszag, 1986) and three differences exist between this turbulence model and standard k–ε: (1) ε equation is solved with an additional term that significantly improves the accuracy for rapidly strained flows; (2) turbulent Prandtl numbers are computed by analytical expressions; (3) effective viscosity is determined by a differential equation. The RNG k–ε governing equations used to calculate k and ε are:

$$\frac{\partial k}{\partial t} + u_j \frac{\partial k}{\partial x_j} = \frac{1}{\rho}\frac{\partial}{\partial x_j}\left(\alpha_k \mu_{\text{eff}} \frac{\partial k}{\partial x_j}\right) + \frac{G_k}{\rho} - \varepsilon, \tag{5}$$

$$\frac{\partial \varepsilon}{\partial t} + u_j \frac{\partial \varepsilon}{\partial x_j} = \frac{1}{\rho}\frac{\partial}{\partial x_j}\left(\alpha_\varepsilon \mu_{\text{eff}} \frac{\partial \varepsilon}{\partial x_j}\right) + \frac{1}{\rho} C_{\varepsilon 1} G_k \frac{\varepsilon}{k} - \left(C_{\varepsilon 2} + \frac{C_\mu \rho \eta^3 \cdot (1 - \eta/\eta_0)}{1 + \beta \eta^3}\right)\frac{\varepsilon^2}{k}, \tag{6}$$

where μ_{eff} is the effective turbulent viscosity; α_k and α_ε are the inverse effective Prandtl number for k and ε; η is Sk/ε; S is the scalar measure of deformation tensor; η_0, β, C_μ, $C_{\varepsilon 1}$ and $C_{\varepsilon 2}$ are constants ($\eta_0 = 4.38$; $\beta = 0.012$; $C_\mu = 0.0845$; $C_{\varepsilon 1} = 1.42$; $C_{\varepsilon 2} = 1.68$) (Chan et al., 2002; Santiago and Martin, 2005).

There are two differences between realizable k–ε and the other k–ε models: (1) a new analytical expression to determine turbulent viscosity where C_μ is no longer a constant, and (2) an equation for ε based on dynamic equation of the mean-square vorticity fluctuation. Actually, the governing equations of realizable k–ε turbulence model are

$$\frac{\partial k}{\partial t} + u_j \frac{\partial k}{\partial x_j} = \frac{1}{\rho}\frac{\partial}{\partial x_j}\left[\left(\mu + \frac{\mu_t}{\sigma_k}\right)\frac{\partial k}{\partial x_j}\right] + \frac{G_k}{\rho} - \varepsilon, \tag{7}$$

$$\frac{\partial \varepsilon}{\partial t} + u_j \frac{\partial \varepsilon}{\partial x_j} = \frac{1}{\rho}\frac{\partial}{\partial x_j}\left[\left(\mu + \frac{\mu_t}{\sigma_\varepsilon}\right)\frac{\partial \varepsilon}{\partial x_j}\right] + C_1 S\varepsilon - C_2 \frac{\varepsilon^2}{k + \sqrt{\nu\varepsilon}}, \tag{8}$$

where $C_1 = \max[0.43, \eta/(\eta + 5)]$; σ_k (= 1.0) and σ_ε (= 1.2) turbulent Prandtl numbers for k and ε respectively; C_2 is a model constant (= 1.9) (Shih et al., 1995; Chan et al., 2002).

2.2. Modelling of interaction of wind with a porous fence

In these cases, a permeable windbreak is considered as a thin porous medium. The physical effect of the presence of a porous fence inside the flow is a pressure drop through it, creating a momentum sink. The pressure change caused by the porous material on incompressible flow can be expressed as $\Delta p = \frac{1}{2} k_r \rho v^2$ (Perry et al., 1997), where v is the normal velocity to porous surface; k_r is the "resistance coefficient" or "pressure loss coefficient". In some cases, the porous fences are characterized by means of porosity, ϕ (defined as the ratio of the area of the holes to the total area).

Thus, for modelling purposes, it is necessary to link resistance coefficient with fence porosity. It can be done using the relationship $k_r = 1.04(1-\phi^2)/\phi^2$ (Reynolds, 1969; Perry et al., 1997; Lee and Lim, 2001). Note that Lee and Lim provided a value of $k_r = 0.52(1-\phi^2)/\phi^2$ due to their definition of k_r that omits the factor of $\frac{1}{2}$ taken into account herein.

3. Bradley and Mulhearn's fence

In past simulation exercises, several studies (Lee and Lim, 2001; Wilson and Yee, 2003) have used the experimental data of Bradley and Mulhearn (1983), denoted B&M data hereafter. Thus, in order to show the possible applicability of the turbulence models used later (standard k–ε, RNG k–ε and realizable k–ε) for solving these cases, we have chosen also B&M data as a benchmark. Here, we only compared experimental and modelled mean flow velocity, while in the IDR/UPM case, studied later in Section 4, a new variable (the peak velocity ratio, defined in Section 4.2) involving velocity and turbulence is analysed. The field data were taken downwind of an isolated porous fence under neutral stability conditions. A windbreak with height $h_b = 1.2$ m was located on a uniform ground with roughness length $z_0 = 0.002$ m ($h_b/z_0 = 600$). In this case, the fence resistance coefficient, necessary for the model simulations, is known ($k_r = 4$, Wilson, 1985; Wilson and Yee, 2003). Thus, it is not necessary to relate porosity with fence resistance coefficient. This 2D configuration has been simulated by using the three different turbulent closure models above mentioned with the same simulation set up representing B&M experiment. The types of boundary conditions are the same used in the IDR/UPM cases (see Section 4.1): wall function at ground, outflow at downstream limit of domain and symmetry at the top. The porous fence is represented as a momentum sink (see Section 2.2). The velocity inlet profile used is a logarithmic profile computed from experimental data. Turbulent kinetic energy and energy dissipation profiles are computed in the same way that for IDR/UPM cases. Numerical domain ranges from $x/h_b = -10$ to 80 in horizontal direction and from $z/h_b = 0$ to 41 in vertical direction with the fence located at $x/h_b = 0$. An irregular Cartesian grid of 90×48 cells was used in domain discretisation. Higher resolution grid ($\Delta x/h_b = 0.125$; $\Delta z/h_b = 0.125$) is employed close to barrier. A grid sensitivity test was performed. A finer mesh with 180×96 cells was used in a simulation for realizable k–ε. The differences between the results obtained with the two grids are below 2%.

In the comparison, streamwise velocity component is normalized with the upwind mean velocity at height $z = 4$ m (u_{04}). Normalized velocity at fixed vertical positions ($z/h_b = 0.38$, 1.88) and the vertical profile of u/u_{04} at $x/h_b = 4.2$ are shown in Fig. 1 comparing B&M measurements and computation results from the present study. Computed normalized velocity for the three turbulence closure models are, overall, in good agreement with the experimental data. Standard k–ε model seems to simulate better the recovery of mean velocity further downstream of the fence at $z/h_b = 0.38$ than the others closures used, but at $z/h_b = 1.88$ not so good results are obtained. Similar behaviour is observed in the results obtained from RNG and realizable k–ε models at these heights underestimating the rate of recovering towards the upstream conditions. In addition, the results concerning the vertical profile at $x/h_b = 4.2$ show that the deceleration at $z/h_b < 1$ and the speed-up above the fence are reproduced by RNG and realizable k–ε models in remarkable good agreement with B&M measurements. Realizable

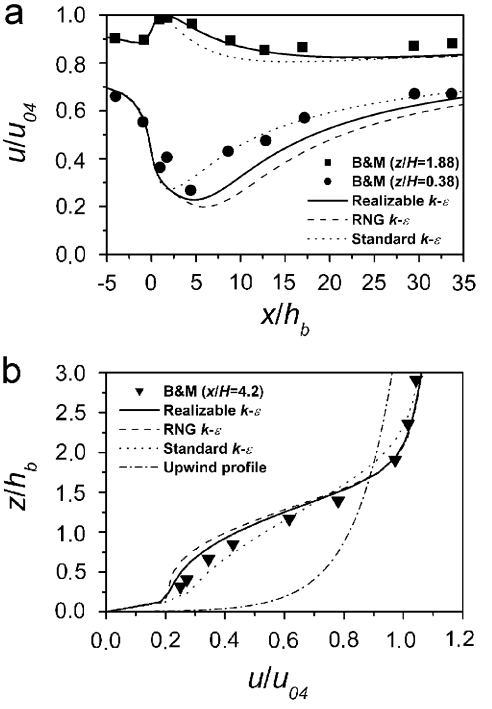

Fig. 1. (a) Horizontal profile of streamwise mean velocity (u/u_{04}) at $z/h_b = 0.38$, 1.88; (b) vertical profile of streamwise mean velocity (u/u_{04}) at $x/h_b = 4.2$.

k–ε shows a slightly better performance. However, the differences amongst the results obtained with different turbulence models are not substantial and all shows an overall good performance to compute mean velocity when using the same numerical method characteristics (grid, domain, etc.).

4. Shelter effect in fences with different porosity

The main objectives of this study are: (1) to find the optimum value of porosity in these conditions based on peak velocity ratio results (defined in Section 4.2), and (2) to evaluate different turbulent closure model performances (standard k–ε, RNG-k–ε and realizable k–ε) using the otherwise identical numerical methods (same grid, domain, boundary conditions, etc.).

4.1. Cases description and experimental and numerical set up

Wind flow around isolated windbreaks has been studied analysing the shelter effect provided by fences. Porosity, related to resistance coefficient as shown in Section 2.2, was used to characterize each windbreak, keeping the values of the others parameter (both geometrical and meteorological) the same in all cases. Thus, the influence of porosity in the shelter zone produced by a windbreak has been analysed in these conditions by changing the porosity of an isolated windbreak. The values of porosity studied were $\phi = 0$ (solid fence), 0.1, 0.24, 0.35, 0.4, 0.5.

4.1.1. Experimental set up

The experiments were carried out in the A9 wind tunnel of IDR/UPM, E.T.S.I. Aeronáuticos, Universidad Politécnica de Madrid. In this facility, a large amount of experimental investigations in the field of wind engineering has been made. Dimensions of the cross section wind tunnel test chamber are $1.4\,\mathrm{m} \times 1.8\,\mathrm{m}$. The porous fences have been built out of perforated plates with circular holes uniformly distributed. They all have a height $h_\mathrm{b} = 0.12\,\mathrm{m}$ and were located on a flat surface. No roughness elements upstream were placed before the test section to create a boundary layer. The wind tunnel inflow velocity profile at the test section was fitted to a logarithmic profile with a $z_0 = 2.4 \times 10^{-14}\,\mathrm{m}$ ($u(z) = (u_*/\kappa)\ln(z/z_0)$, where u_* is the friction velocity ($0.3\,\mathrm{m\,s^{-1}}$)). The streamwise velocity profiles obtained are almost flat, except inside a narrow zone close to the ground where the velocity rapidly grows from zero at the wall to reach the nominal speed. Most of the previous investigations have studied cases with larger values of roughness length (e.g. $h_\mathrm{b}/z_0 = 600$ in Bradley and Mulhearn (1983); $h_\mathrm{b}/z_0 = 160$ in Wilson (1997), where h_b is barrier height), but in this work we are interested in the shelter effect of windbreaks located in harbours, and even though the roughness length used in these cases is lower, we are interested in analysing an extreme case with upwind profiles quasi-constant with height for streamwise velocity (z_0 almost 0). However, the reader should bear in mind that even a smooth surface has not a roughness length of 0 and in real situations can never reach this value. The blockage ratio parameter, defined as the ratio of the projected frontal area of the object placed in the wind tunnel to the area of the test section, is around 6.6% in the experimental case of the solid barrier. This parameter should be less than 5% to ensure the aerodynamical independence of flow pattern, and following Barlow et al. (1999) a correction of $\frac{1}{4}$ of blockage ratio should be computed. However, in this case the correction is below 2% and it is considered negligible. Velocity and turbulence measurements behind the fences were performed by using one component Dantec Streamline 90N10 Frame hot wire anemometer.

4.1.2. Numerical set up

A CFD simulation was set up to represent the wind tunnel experiment. The inlet velocity profile used in the simulations corresponds to the logarithmic profile described above. However, we have not experimental data about inlet profiles of turbulent kinetic energy, k_in, and energy dissipation, ε_in. Thus, the inlet boundary conditions for the turbulent kinetic energy and its dissipation rate have been obtained from the assumption of an equilibrium boundary layer,

$$k_\mathrm{in} = \frac{u_*^2}{\sqrt{C_\mu}} = 0.3\,\mathrm{m^2\,s^{-2}} \quad \text{and} \quad \varepsilon_\mathrm{in} = (C_\mu^{3/4} k_\mathrm{in}^{3/2})/\kappa z,$$

where κ is von Karman's constant ($\kappa = 0.4$) (Richards and Hoxey, 1993; Versteeg and Malalasekera, 1995; Santiago and Martin, 2005). The Reynolds number based on fence height was approximately 1.9×10^5.

At ground, standard wall functions have been used. Porous fences have been represented as a momentum sink (see Section 2.2), but in the case of

a solid barrier a standard wall function has been used. At the upper boundary, zero normal velocity and zero normal gradients of all variables have been imposed and at the downstream limit of the domain the flow has been considered fully developed (outflow). The same 2D numerical domain was used in all simulations. In the streamwise direction, it ranges from $x/h_b = -50$ to 100 with the barrier located at $x/h_b = 0$. The height of the domain used is $30h_b$ leading to a blockage ratio around 3.3%. Also, simulations with $70h_b$ have been performed and negligible changes in the results (<1% in the maximum of velocity near the windbreak) have been found. Therefore, a domain height of $30h_b$ was considered high enough to simulate the flow around windbreak without being affected by the boundary conditions imposed at $z = 30h_b$. The mesh was also the same in all simulations. An irregular mesh is used: near the fence the grid size is $0.015\,\text{m} \times 0.015\,\text{m}$ ($\Delta x/h_b = 0.125$; $\Delta y/h_b = 0.125$) and it is increased away from the fence. The Cartesian grid size is 80×30 cells (GRID 1). A test of the cell size effect has been performed to check whether the grid resolution is influencing the model results. To do so a finer grid with 160×60 cells ($\Delta x/h_b = 0.0625$; $\Delta y/h_b = 0.0625$ near the fence) called GRID 2 and a coarser grid with 40×15 cells ($\Delta x/h_b = 0.25$; $\Delta y/h_b = 0.25$ near to the fence) called GRID 3 were also used. There is no need to make the grid sensitivity test for more than one turbulence model, thus the test has been performed using the results of realizable k–ε model for the solid fence case. Fig. 2 shows peak velocity ratio $R_u^1(x,z)$, (parameter defined in Eq. (9)), behind the solid fence obtained with the three grids at $z/h_b = 1$ and 4 for realizable k–ε. Small differences (<1%) are observed for the finer grids (GRID 1 and 2). Higher differences are found for the coarse grid (GRID 3). Therefore, results show that the spatial resolution of GRID 1 is enough to obtain correct grid-independent simulations of air flows around the windbreak.

The model governing equations is solved by using a collocated grid system by the finite volume method. Discretised equations are solved by the segregated method. In order to avoid numerical error of first order discretisation methods, a second-order upwind scheme was used. To solve the pressure–velocity coupling the SIMPLE (semi-implicit method for pressure-linked equations) method, described by Patankar (1980), has been employed. The SIMPLE algorithm is adequate since it has been widely used for atmospheric flows, for example in street canyon modelling (Kim and Baik, 1999; Chan et al., 2002) or flow around windbreaks (Wilson, 1985). Concerning the convergence criteria, the residual values dropped below 10^{-9} in all simulations.

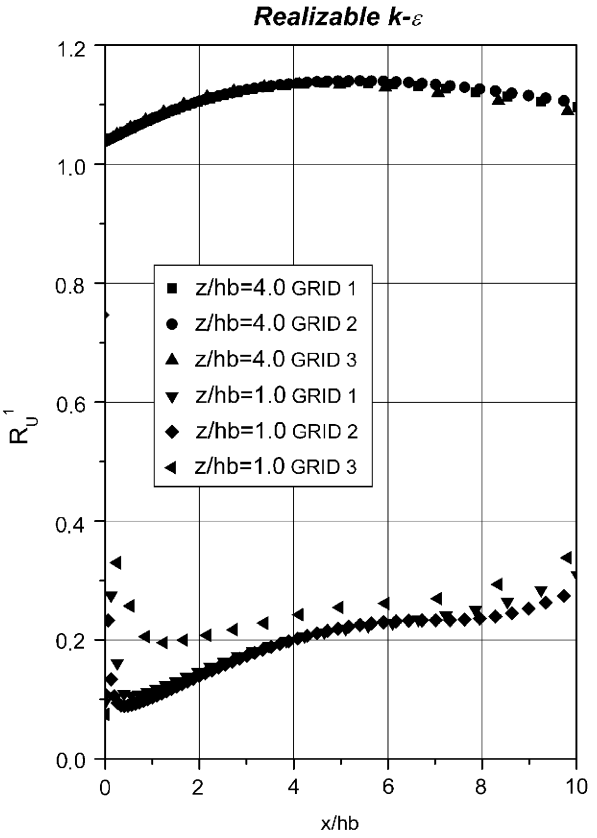

Fig. 2. Peak velocity ratio, $R_u^1(z)$, at vertical positions $z/h_b = 1$ and 4 behind a solid fence of height h_b. x is distance from the fence; z is vertical position. GRID 1 is the mesh with 80×30 cells, GRID 2 with 160×60 cells and GRID 3 with 40×15 cells.

4.2. Results and discussions

4.2.1. Evaluation of turbulence models and parameters used

The principal effect of a windbreak is to reduce wind velocity, which can be splitted into two components: average velocity and turbulent fluctuation. Some studies compare independently average and turbulent components (e.g. Packwood, 2000 found better results in numerical simulations for mean velocity than for turbulence parameters). However, in this work we intend to summarize the information of the shelter zone created in just one

parameter defined as the peak velocity ratio:

$$R_u^1(x,z) = \frac{U(x,z) + \sigma(x,z)}{U_{\text{ref}} + \sigma_{\text{ref}}}, \tag{9}$$

where $U(x,z)$ is mean velocity and $\sigma(x,z)$ is velocity standard deviation. The peak velocity is assumed to be $U(x,z)+\sigma(x,z)$. This parameter takes into account both the mean value and the turbulent fluctuation. Subscript "ref" indicates reference values at $z/h_b = 6.67$ upstream from the fence. The peak velocity for disturbed flow is compared with that for undisturbed flow. Peak velocity ratio provides similar information than protection factor ($1/R_u^1(x,z)$) introduced by Gandemer (1979) and it was also used by Frank and Ruck (2005) as pedestrian comfort parameter.

The peak velocity ratio profiles obtained from wind tunnel measurements and from numerical simulations downstream of fences with different porosity, ϕ: 0 (solid fence), 0.1, 0.24, 0.35, 0.4, 0.5 are shown in Figs. 3–8. The evaluation of the turbulence models is based on the comparison among computed peak velocity ratio and wind tunnel data. So called "verification" of the models is carried out by using the following statistical performance parameters: root mean square (RMS), fractional bias (FB) and correlation coefficient (R). Definitions can be found in Wilks (1995)

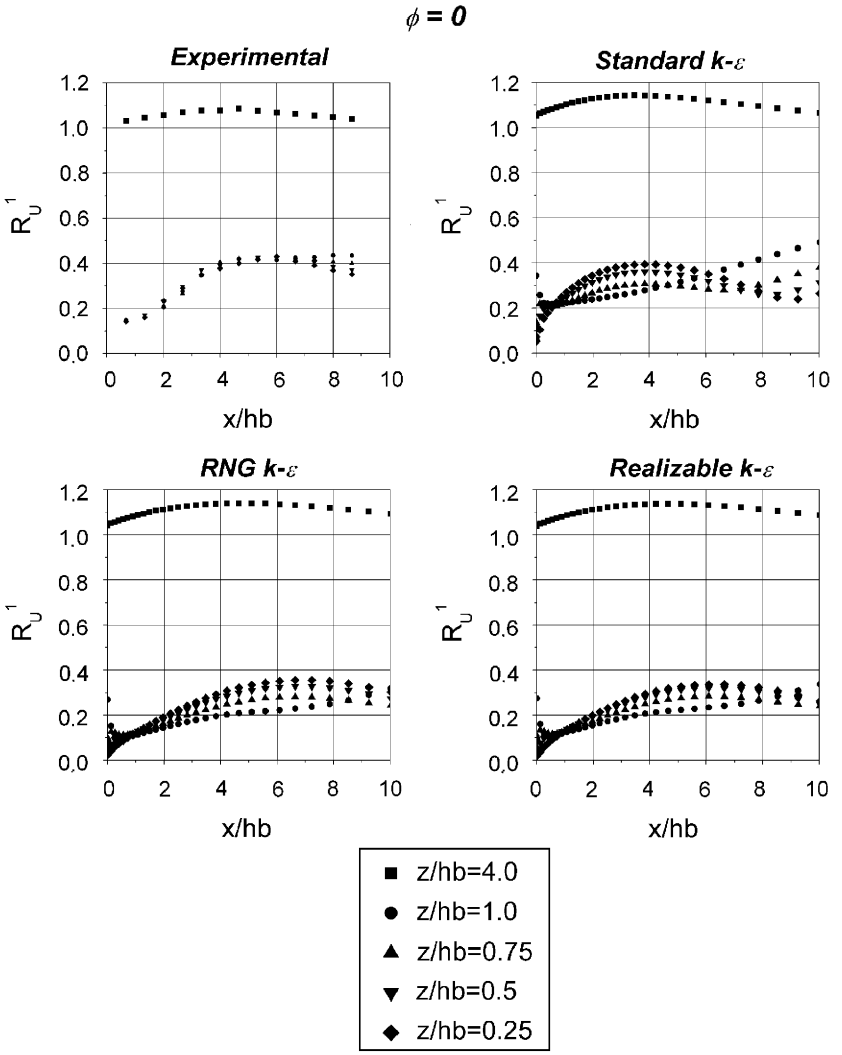

Fig. 3. Experimental and numerical peak velocity ratio profiles, $R_u^1(z)$, at several vertical positions ($z/h_b = 0.25, 0.5, 0.75, 1, 4$) behind a solid fence, obtained for different turbulence models. h_b, x, z and ϕ are fence height, distance from the fence, vertical position and porosity, respectively.

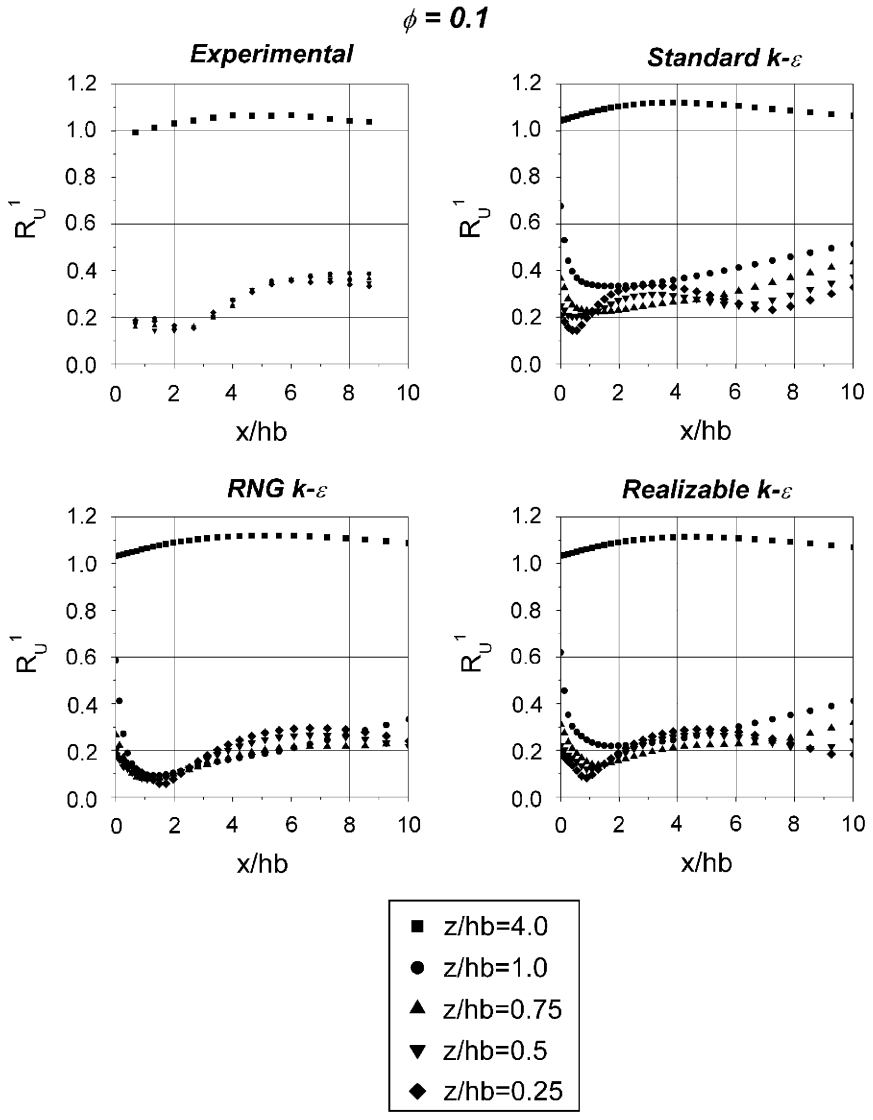

Fig. 4. As Fig. 3 with porosity $\phi = 0.1$.

and Hanna et al. (1991)

$$\mathrm{RMS} = \left[\sum_{\text{points}} \frac{(R^1_{u\mathrm{EXP}} - R^1_{u\mathrm{COM}})^2}{N}\right]^{1/2}, \tag{10}$$

$$\mathrm{FB} = \frac{\overline{R^1_{u\mathrm{EXP}}} - \overline{R^1_{u\mathrm{COM}}}}{0.5 \cdot (\overline{R^1_{u\mathrm{EXP}}} + \overline{R^1_{u\mathrm{COM}}})}, \tag{11}$$

$$R = \frac{\sum_{\text{points}} \left[(R^1_{u\mathrm{EXP}} - \overline{R^1_{u\mathrm{EXP}}})(R^1_{u\mathrm{COM}} - \overline{R^1_{u\mathrm{COM}}})\right]}{\left[\sum_{\text{points}} (R^1_{u\mathrm{EXP}} - \overline{R^1_{u\mathrm{EXP}}})^2\right]^{1/2} \left[\sum_{\text{points}} (R^1_{u\mathrm{COM}} - \overline{R^1_{u\mathrm{COM}}})^2\right]^{1/2}}, \tag{12}$$

where N is the number of data points, $R^1_{u\mathrm{EXP}}$ and $R^1_{u\mathrm{COM}}$ are observed and predicted values, respectively, whereas $\overline{R^1_{u\mathrm{EXP}}}$ and $\overline{R^1_{u\mathrm{COM}}}$ are the respective mean value. RMS shows the dispersion between computed and experimental results. Negative or positive FB gives information about over- or underestimation of models, respectively. Finally, correlation among simulation and wind tunnel experiment data are determined by R.

Statistical performance parameters (Eqs. (10)–(12)) at $z/h_b \leqslant 1$ (region of interest) are calculated and analysed and its values are summarized in Table 1. Table 1 and Figs. 3–8 suggest that the

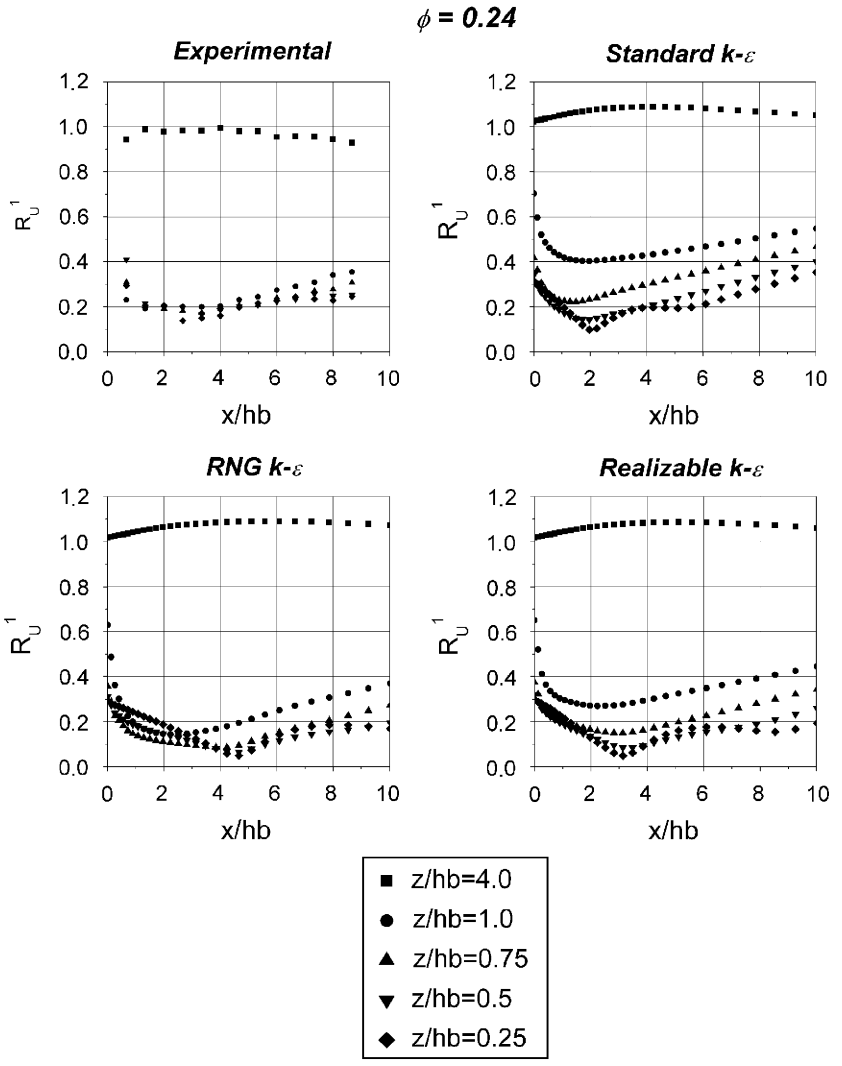

Fig. 5. As Fig. 3 with porosity $\phi = 0.24$.

performance of any of these models against the wind tunnel data is not particularly good. However, in general, the agreement of RNG k–ε and realizable k–ε turbulence models with experimental measurements is acceptable, although $R_u^1(x,z)$ values at $z/h_b \leqslant 1$ are, generally, slightly underestimated especially for RNG. Standard k–ε results are worse than those other turbulence models. It overestimates $R_u^1(x,z)$ values indicated by negative values of FB. This fact can be due to the fact that standard k–ε presents an overprediction of turbulent kinetic energy near building edges (Chan et al., 2003). Standard k–ε provides, generally, the highest values of RMS and poor correlations which can be related to its general inaccuracy for flows with adverse pressure gradient and the underprediction of the size of the recirculating zones in some cases (Sini et al., 1996). This fact can explain the underestimation of the distance between the fence and the minimum of $R_u^1(x,z)$ for this turbulence model in Figs. 3–5. In the case of $\phi = 0$ the windbreak is simulated as smooth wall. In all cases there are not experimental measurements very close to the fence ($x/h_b = 0$) and the first experimental data is for $x/h_b = 0.667$. Thus, the turbulence models cannot be tested very close to the fence, and the numerical results obtained there should be observed carefully. In the case of $\phi = 0$, the performance of the turbulence models in this zone could be probably improved by using others more complex treatments near the wall or using a low Reynolds turbulence model like k-omega.

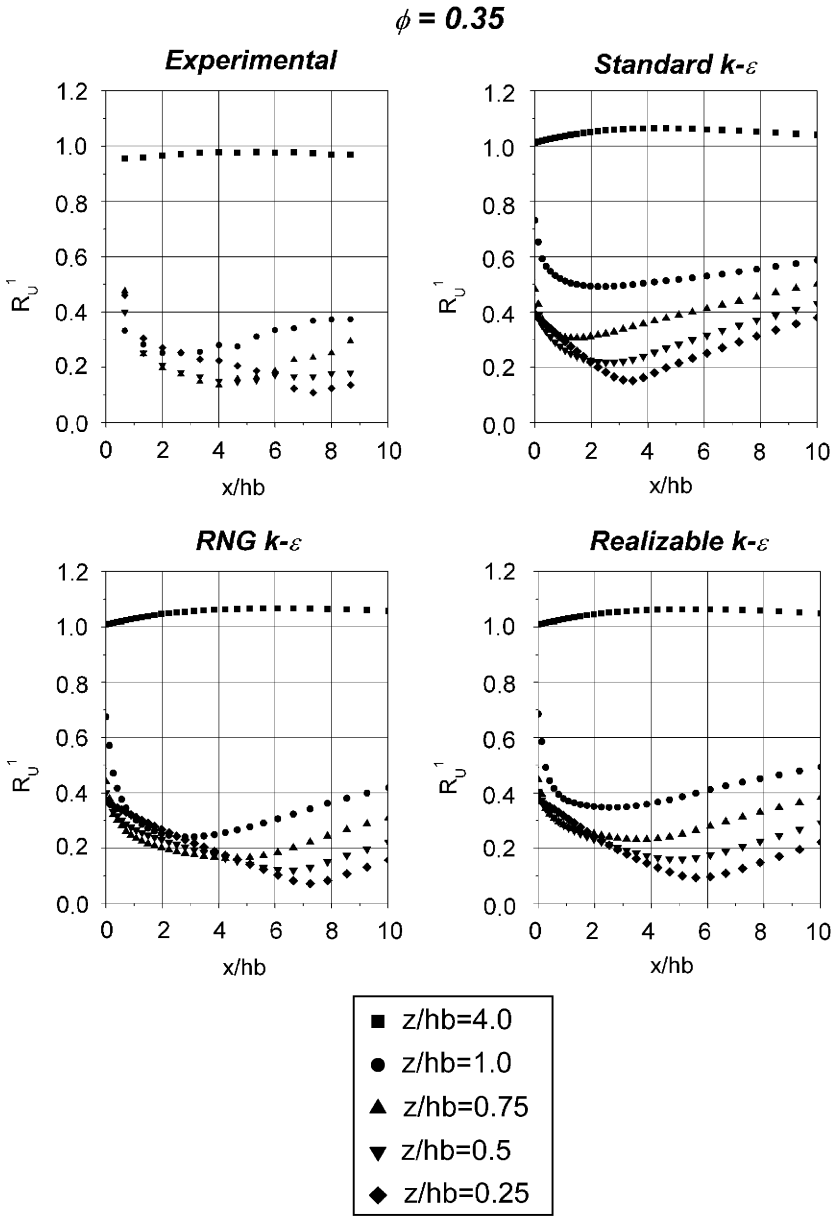

Fig. 6. As Fig. 3 with porosity $\phi = 0.35$.

In general, the RNG and realizable k–ε turbulence models provide better results than the standard one, because of their modifications for adverse pressure gradient flows. The modification inside ε equation of RNG k–ε produces decreasing of k in large strain rate zones, and hence a better estimation of recirculating zones. For this turbulence model, R values are the best values obtained (close to 1) but FB computed have rather large positive values indicating that RNG simulate well the shape of the recirculation zone but with a systematic underestimation of the intensity of the wind. In addition, the obtained RMS values are generally good but they have slightly larger values than realizable k–ε results. The realizable k–ε modifications (C_μ is no longer a constant) solves some standard k–ε problems, such as the possible violation of Schwartz inequality for shear stress where there are large strain rates. This turbulence model provides, overall, the best RMS and FB data among the turbulence models studied, but a slight tendency towards the underestimation of peak velocity have

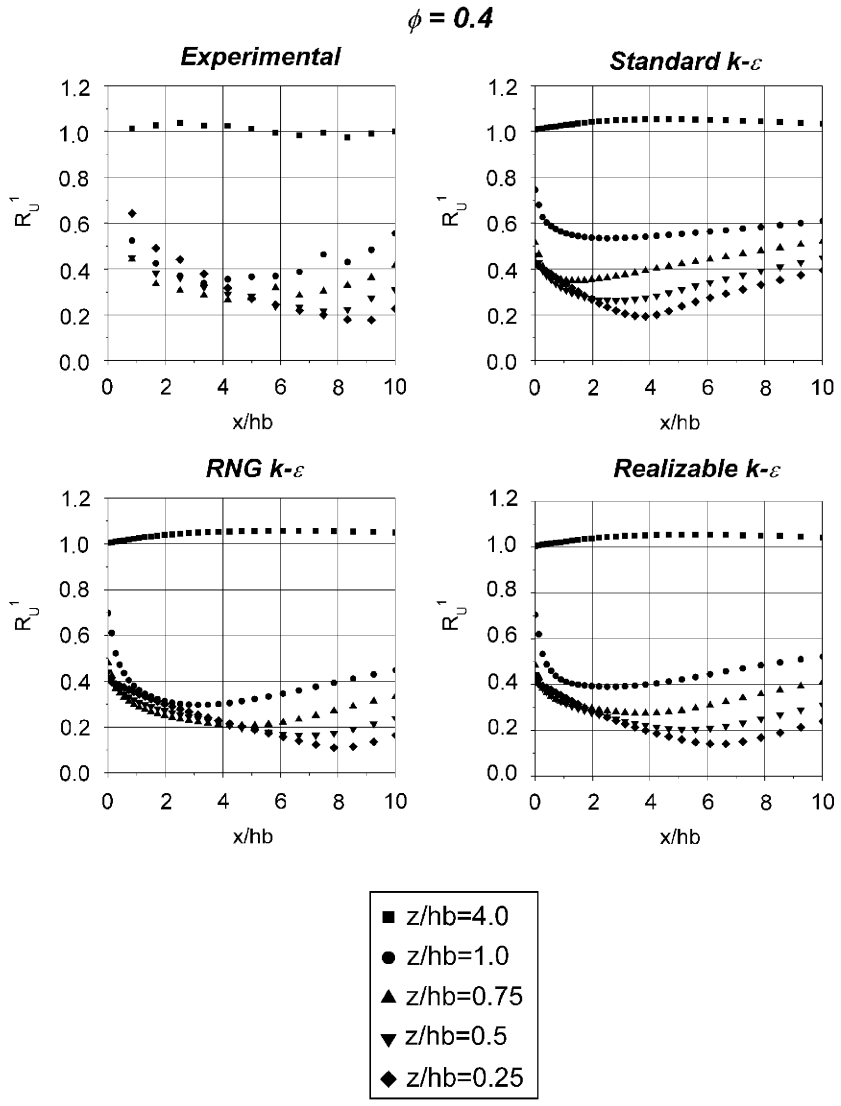

Fig. 7. As Fig. 3 with porosity $\phi = 0.4$.

been observed (but less than in the case of the RNG k–ε model). Values of R for realizable k–ε are smaller than those obtained with RNG k–ε, but, nevertheless, these values can be considered acceptable. As commented above, the standard k–ε performs worse than the other two turbulence models. Hence herein we are going to focus the discussion on RNG and realizable k–ε. From Figs. 3–8, we can observe that the RNG and realizable k–ε turbulence models seem to have better performance for large porosities ($\phi \geqslant 0.35$), especially in the far lee field $x/h_b \geqslant 4$ and no great discrepancies are found between them. Most of the differences in the value of peak velocity ratio can be attributed to the computation of turbulent kinetic energy because mean velocity is well estimated as presented in Section 3 and as found by Packwood (2000). For these cases, it has been checked (not shown in this paper) that RNG k–ε produces lower values of turbulent kinetic energy than realizable k–ε, explaining the lower value of peak velocity ratio that is generally found. For the studied cases with low porosity ($\phi \leqslant 0.24$) near the fence, the estimation of the size of recirculation zone has an influence on the peak velocity ratio values and the realizable k–ε provides a better solution in the reattachment length (García Sagrado et al., 2002). It is interesting to analyse the discrepancies between peak velocity ratio computed by RNG and realizable k–ε turbulence models and experimental values

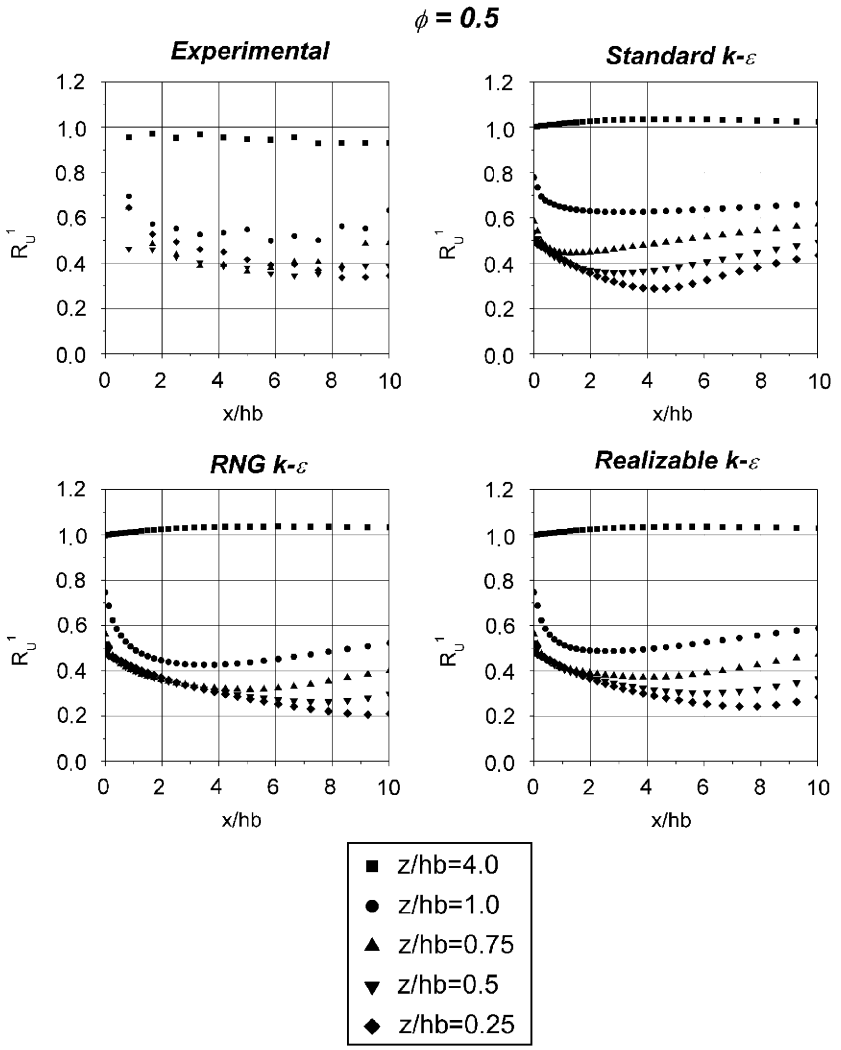

Fig. 8. As Fig. 3 with porosity $\phi = 0.5$.

in the far lee field. Then, we can observe the evolution of peak velocity ratio with porosity, as shown in Fig. 9 where experimental and numerical peak velocity ratio versus fence porosity at $x/h_b = 8$ for $y/h_b = 1$ and 0.5 are plotted. It is observed, as commented before, the better performance of both turbulence models is for large porosities. In conclusion, RNG and realizable k–ε have similar performances in this case study and their results improve those provided by standard k–ε. Thus, in some situations, it can be suitable to use both models.

4.2.2. Optimum porosity

In this section the objective is to determine, among the values of porosity considered, the porosity value which provides the largest shelter zone behind the fence. For this purpose, experimental measurements are analysed at heights less than h_b ($z/h_b < 1$). In the solid fence case ($\phi = 0$) $R_u^1(x, z)$ values are between 0.15 and 0.3 near the fence ($x/h_b < 4$) and are almost constant and close to 0.4 from $x/h_b = 4$ to 10. The solid fence provides a sheltered zone very close to it but its protection at larger distances is not so good due to the re-circulating bubble that appears behind the fence. A larger protection distance is given by the porous fence with $\phi = 0.1$. $R_u^1(x, z)$ values are between 0.15 and 0.3 in the range of $x/h_b < 5$ and are almost constant (close to 0.4) from $x/h_b = 6$ to $x/h_b = 10$. A re-circulating flow region appears in the leeward side of the barrier. In the case of porosity $\phi = 0.24$, $R_u^1(z)$ has values between 0.1 and 0.3 when the

Table 1
Root mean square, fractional bias and correlation coefficient between experimental and numerical $R_u^1(z)$ values, computed for three turbulence models (Standard k–ε, RNG k–ε and Realizable k–ε) at $z/h_b \leqslant 1$ and for different windbreak porosities

	Standard k–ε			RNG k–ε			Realizable k–ε		
	RMS	FB	R	RMS	FB	R	RMS	FB	R
$\phi = 0$	0.087	0.122	0.456	0.119	0.343	0.750	0.120	0.357	0.795
$\phi = 0.1$	0.092	−0.091	0.358	0.098	0.366	0.878	0.080	0.173	0.664
$\phi = 0.24$	0.119	−0.307	0.704	0.077	0.352	0.815	0.063	0.083	0.779
$\phi = 0.35$	0.169	−0.479	0.594	0.027	0.062	0.949	0.067	−0.156	0.841
$\phi = 0.4$	0.139	−0.232	0.479	0.079	0.244	0.927	0.069	0.053	0.776
$\phi = 0.5$	0.098	−0.081	0.619	0.101	0.242	0.913	0.076	0.128	0.827

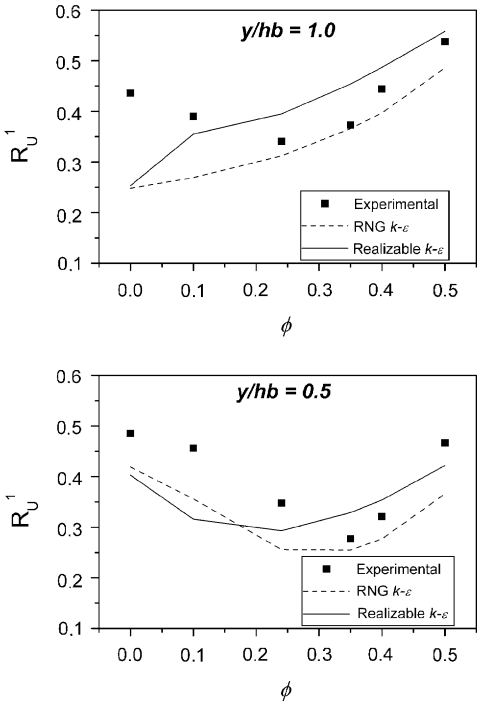

Fig. 9. Experimental and numerical peak velocity ratio versus fence porosity at $x/h_b = 8$ for $y/h_b = 1$ and 0.5.

distance from the barrier is in the range $0.5 < x/h_b < 10$. Re-attachment point seems to be moved downstream by the effect of the flow passing through the barrier. This porous fence provides a better shelter at larger distances than barriers with less porosity. When fence porosity is $\phi = 0.35$, $R_u^1(x,z)$ has experimental values between 0.1 and 0.4 for distances from the barrier in the range $0.5 < x/h_b < 5$. In addition, at $z/h_b = 0.5$ and 0.25, $R_u^1(x,z)$ has values lower than 0.3 for $x/h_b > 2$, producing a better protection for larger distances than the previous cases (fences with less porosity). Moreover, for $x/h_b > 6$, the shelter effect decreases (higher values of $R_u^1(x,z)$) as z/h_b increases. In this case and for fences with higher porosity, the re-circulating region disappears. However, in higher porosity cases the shelter effect is not so effective. For porosity $\phi = 0.4$ or larger, the protection far from the fence is better than close to it. But this protection is not as good as the shelter provided by the previous case ($\phi = 0.35$), since $R_u^1(x,z)$ has values between 0.2–0.3 for $z/h_b = 0.25$ and 0.5. In addition, worse protection for large distance (higher values of $R_u^1(x,z)$) is also detected when z/h_b increases. Finally, the fence with porosity $\phi = 0.5$ seems to have a similar behaviour than $\phi = 0.4$ case, but with higher values of $R_u^1(x,z)$ (0.6–0.3 for $z/h_b = 0.25$ and 0.5). In conclusion, a porosity $\phi = 0.35$ is found to be the best value, relative to study range, to provide an effective shelter effect in these conditions with a flat streamwise velocity profile, even at large distance. In addition, at short and intermediate distances, the shelter effect observed is similar to the one produced by a fence with less porosity. Similar conclusion can be obtained analysing the numerical results. A fence with a similar value of porosity (0.3) was found by Park and Lee (2002) to be useful for reducing the wind speed without the formation of a re-circulating bubble behind the fence in an open storage of coal piles.

5. Conclusions

The flow around a windbreak located on a flat surface (roughness length almost 0) has been investigated by numerical and experimental studies. The shelter effect produced by an isolated porous fence has been analysed in terms of the peak velocity

parameter ($R_u^1(x,z)$), focusing on the fence porosity that produces the largest protection region.

The differences in terms of mean velocity among the three turbulent closure models and B&M results considered are not very large. Larger differences are found between numerical results for the three closures and IDR/UPM cases, probably because a smaller area of study is considered ($x/h_b<10$) and more points in this region are compared. In addition, turbulence is considered in the parameter study, peak velocity ratio. For IDR/UPM cases, the performance of RNG and realizable k–ε is acceptable and clearly better than the standard k–ε one. Hence, this type of simulations can be useful for studies such as the analysis of sheltering effect of a porous fence. In future studies, other turbulence models like k-omega or RSM models could be used to try to improve the representation of the peak velocity. Additionally, k–ε turbulence models with modified constant for atmospheric boundary layer could also be used. In this regard it is important to note that Milliez and Carissimo (2007) found that the original numerical values for the coefficients of standard k–ε, are the most adapted to local scale simulations for an array of buildings.

The best windbreak porosity for an efficient downwind shelter in these conditions is $\phi = 0.35$ as confirmed by the experimental results. It provides the best shelter at large distance and, in short and intermediate distances, it produces a similar protection to a fence with less porosity. The barriers studied with less porosity seem to present a recirculating flow region at downstream. Therefore, the windbreak recommended to protect piles of materials stored in an open location in harbours is a porous fence with porosity close to 0.35 because it shows the most reduced peak velocity ratio value at large distance downstream from the fence. Other studies with higher z_0 recommend a similar porosity values (Park and Lee, 2002), therefore the roughness length does not seem to have a significant effect on the conclusions drawn in this paper.

Barlow, J.B., Rae, W.H., Pope, A., 1999. Low-speed Wind Tunnel Testing. Wiley, New York.

Borges, A.R., Viegas, D.X., 1988. Shelter effects on a row of coal piles to prevent wind erosion. Journal of Wind Engineering and Industrial Aerodynamics 29, 145–154.

Bradley, B.F., Mulhearn, P.J., 1983. Development of velocity and shear stress distributions in the wake of porous shelter fence. Journal of Wind Engineering and Industrial Aerodynamics 15, 145–156.

Chan, T.L., Dong, G., Leung, C.W., Cheung, C.S., Hung, W.T., 2002. Validation of a two dimensional pollutant dispersion model in an isolated street canyon. Atmospheric Environment 36, 861–872.

Chan, A.T., Au, W.T.W., So, E.S.P., 2003. Strategic guidelines for street canyon geometry to achieve sustainable street air quality—part II: multiple canopies and canyons. Atmospheric Environment 37, 2761–2772.

Dyrbye, C., Hansen, S.O., 1997. Wind Effect on Structures. Wiley, New York.

Frank, C., Ruck, B., 2005. Double-arranged mound-mounted shelterbelts: influence of porosity on wind reduction between the shelters. Environmental Fluid Mechanics 5, 267–292.

Gandemer, J., 1979. Wind shelters. Journal of Industrial Aerodynamics 4, 371–389.

Gao, Z., Wang, J., Ma, Y., Kim, J., Choi, T., Lee, H., Asanuma, J., Su, Z., 2000. Study of roughness lengths and drag coefficients over Nansha Sea Region, Gobi Desert, Oasis and Tibetan Plateau. Physics and Chemistry of the Earth (B) 25, 141–145.

Garcia Sagrado, A.P., van Beeck, J., Rambaud, P., Olivari, D., 2002. Numerical and experimental modelling of pollutant dispersion in a street canyon. Journal of Wind Engineering and Industrial Aerodynamics 90, 321–339.

Hanna, S.R., Strimaitis, D.G., Chang, J.C., 1991. Hazard response modelling uncertainty (a quantitative method) Volume II. Evaluation of commonly used hazardous gas dispersion model. Report F08635-89-C-0136, Sigma Research Corporation, Air Force Engineering and Service Center, Tyndal Air Force Base, Florida.

Jensen, K., Koss, H., Soendergaard, T., 2001. Feasibility study of windscreens in harbours. Proceedings of the Third European and African Conference on Wind Engineering, Eindhoven, The Netherlands.

Judd, M.J., Raupach, M.R., Finnigan, J.J., 1996. A wind tunnel study of turbulent flow around single and multiple windbreaks, Part I: velocity fields. Boundary Layer Meteorology 80, 127–165.

Kim, J.-J., Baik, J.-J., 1999. A numerical study of thermal effects on flow and pollutant dispersion in urban street canyons. Journal of Applied Meteorology 38, 1249–1261.

Launder, B.E., Spalding, D.B., 1974. The numerical computation of turbulent flow. Computational Methods in Applied Mechanical Engineering 3, 269–289.

Lee, S.J., Lim, H.C., 2001. A numerical study on flow around a triangular prism located behind a porous fence. Fluid Dynamics Research 28, 209–221.

McAneney, K.J., Judd, M.J., 1991. Multiple windbreaks: an aeolean ensemble. Boundary Layer Meteorology 54, 129–146.

Milliez, M., Carissimo, B., 2007. Numerical simulations of pollutant dispersion in an idealized urban area, for different

meteorological conditions. Boundary Layer Meteorology 122, 321–342.
Packwood, A.R., 2000. Flow through porous fences in thick boundary layers: comparison between laboratory and numerical experiments. Journal of Wind Engineering and Industrial Aerodynamics 88, 75–90.
Park, C.W., Lee, S.J., 2002. Verification of the shelter effect of a windbreak on coal piles in the POSCO open storage yards at the Kwang–Yang works. Atmospheric Environment 36, 2171–2185.
Patankar, S.V., 1980. Numerical Heat Transfer and Fluid Flow. Hemisphere Publishing Corporation, New York.
Perera, M.D.A.E.S., 1981. Shelter behind two-dimensional solid and porous fences. Journal of Wind Engineering and Industrial Aerodynamics 8, 93.
Perry, R.H., Green, D.W., Maloney, J.O., 1997. Perry's Chemical Engineers' Handbook. Mc Graw-Hill, New York.
Plate, E.J., 1971. The aerodynamics of shelter belts. Agricultural Meteorology 8, 203–222.
Raine, J.K., Stevenson, D.C., 1977. Wind protection by model fences in a simulated atmospheric boundary layer. Journal of Industrial Aerodynamics 2, 159–180.
Reynolds, A.J., 1969. Flow deflection by gauze screens. Journal of Mechanical Engineering Science 11, 290.
Richards, P.J., Hoxey, R.P., 1993. Appropriate boundary conditions for computational wind engineering models using the k-ε turbulence model. Journal of Wind Engineering and Industrial Aerodynamics 46 & 47, 145–153.
Santiago, J.L., Martin, F., 2005. Modelling the air flow in symmetric and asymmetric street canyons. International Journal of Environment and Pollution 25, 145–154.
Shih, T.H., Liou, W.W., Shabbir, A., Zhu, J., 1995. A new k–ε eddy-viscosity model for high Reynolds numbers turbulent flows—model development and validation. Computers Fluids 24, 227–238.
Tani, N., 1958. On the wind tunnel test of the model shelter-hedge. Bulletin of the National Institute of Agricultural Sciences Series A 6, 75–80.
Versteeg, H.K., Malalasekera, W., 1995. An Introduction to Computational Fluid Dynamics. The Finite Volume Method, Pearson Prentice-Hall, Harlow.
Wang, H., Takle, E.S., 1995. A numerical simulation of boundary layer flows near shelterbelts. Boundary Layer Meteorology 75, 141–173.
Wilks, D.S., 1995. Statistical Methods in Atmospheric Sciences. Academic Press, San Diego.
Wilson, J.D., 1985. Numerical studies of flow through a windbreak. Journal of Wind Engineering and Industrial Aerodynamics 21, 119–154.
Wilson, J.D., 1997. A field study of the mean pressure about a windbreak. Boundary Layer Meteorology 85, 327–358.
Wilson, J.D., 2004a. Oblique, stratified winds about a shelter fence. Part I. measurements. Journal of Applied Meteorology 43, 1149–1167.
Wilson, J.D., 2004b. Oblique, stratified winds about a shelter fence. Part II: comparison of measurements with numerical models. Journal of Applied Meteorology 43, 1392–1409.
Wilson, J.D., Mooney, C.J., 1997. A numerical simulation of boundary-layer flows near shelterbelts-comments. Boundary-Layer Meteorology 85, 137–149.
Wilson, J.D., Yee, E., 2003. Calculation of wind disturbed by an array of fences. Agricultural and Forest Meteorology 115, 31–50.
Yakhot, V., Orszag, S.A., 1986. Renormalization group analysis of turbulence: I. basic theory. Journal of Scientific Computing 1, 1–51.